Available online at www.sciencedirect.com
SCIENCE DIRECT®
Geothermics 34 (2005) 495–517
GEOTHERMICS
www.elsevier.com/locate/geothermics

Chemical and isotope characteristics of the Chachimbiro geothermal fluids (Ecuador)

Eduardo Aguilera [a], Roberto Cioni [b,*], Fabrizio Gherardi [b], Gabriella Magro [b], Luigi Marini [c], Zhonghe Pang [d]

[a] *Escuela Politécnica del Ejército (ESPE), Campus Politécnico, Av. El Progreso s/n, Sangolquí, Ecuador*
[b] *Istituto di Geoscienze e Georisorse, Area della Ricerca CNR, Via Moruzzi 1, 56124 Pisa, Italy*
[c] *Dip.Te.Ris., University of Genova, Corso Europa 26, 16132 Genova, Italy*
[d] *International Atomic Energy Agency, Wagramer Strasse 5, Vienna, Austria*

Received 16 December 2002; accepted 22 April 2005
Available online 27 June 2005

Abstract

The parent geothermal water proposed for the Chachimbiro geothermal area has calculated values of 2250 mg/L Cl and approximately 5 bar P_{CO_2}. It comes from a reservoir having an estimated temperature of 225–235 °C, although temperatures somewhat higher than 260 °C may be present at the roots of the system. The geothermal reservoir at Chachimbiro is recharged mainly by meteoric water (about 92%) and secondarily by arc-type magmatic water. Carbon and sulfur isotope data support a magmatic origin for the C and S species entering the geothermal system from below, consistent with indications provided by He isotopes.

The thermal springs of Na–Cl to Na–Cl–HCO_3 type located in the Chachimbiro area originate through dilution of the parent geothermal water and have reached different degrees of re-equilibration with country rocks at lower temperatures.

Keywords: Isotopes; Geochemistry; Thermal springs; Chachimbiro; Ecuador

* Corresponding author. Fax: +39 050 3152323.
E-mail address: cioni@igg.cnr.it (R. Cioni).

0375-6505/$30.00 © 2005 CNR. Published by Elsevier Ltd. All rights reserved.
doi:10.1016/j.geothermics.2005.04.004

1. Introduction

The Chachimbiro geothermal area is located in the Western Andean Range (Cordillera Occidental), about 70 km NNE of Quito and 17 km NE of Ibarra (Fig. 1a). The center of the area of interest is at 0°25′N and 78°17′W, at an average elevation of 2560 m above sea level (m asl). The rough topography is dominated by the Cotocachi (4944 m asl) and Yanahurcu de Piñan (4535 m asl) stratovolcanoes (Fig. 1b).

Previous geochemical investigations at Chachimbiro to assess the geothermal potential of the area were carried out within the framework of OLADE-INECEL (unpublished report), OLADE-AQUATER (unpublished report) and IAEA-INECEL (Almeida et al., 1992) projects. Some 20 samples of thermal and cold waters were collected and analysed for major chemical components, δD and δ^{18}O values, and tritium activity. Based on these data, the area appeared to be of considerable geothermal interest and worthy of further investigation (Almeida et al., 1992). This paper discusses the results of the geochemical and isotopic investigations conducted in June 1999 and July 2001, as well as the results from previous studies, and also presents an updated conceptual geochemical model of the Chachimbiro geothermal area.

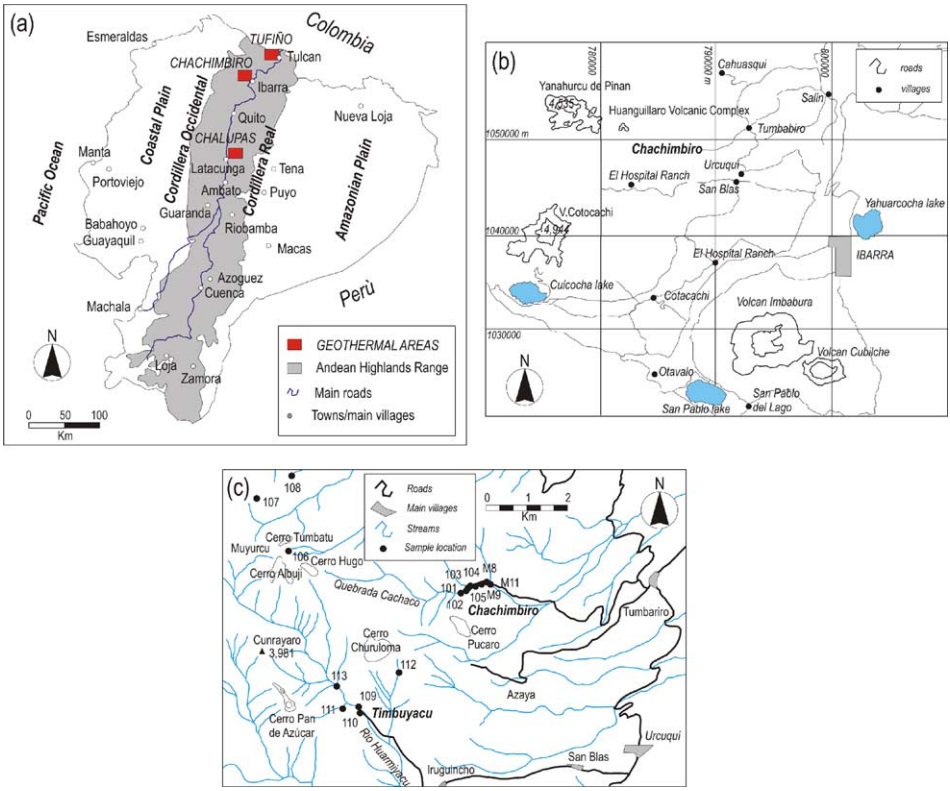

Fig. 1. Map of the Chachimbiro geothermal area showing the location of sampled springs.

2. Geological framework

The geodynamics of Ecuador is dominated by the subduction of the Nazca Plate beneath the South American Plate. The Andean Cordillera in Ecuador consists of two parallel mountain ranges, the Cordillera Occidental in the west and the Cordillera Real in the east, separated by the almost flat Inter-Andean Depression (Aguilera, 1998). The western range is composed mainly of basic and intermediate volcanics, emplaced in a submarine environment and covered by discontinuous turbidite deposits, while the eastern range consists of metamorphosed intrusive and sedimentary rocks. The Inter-Andean Depression is a tensional structure of regional importance bounded by active normal faults and filled with volcanic and volcano-sedimentary deposits that can reach a thickness of several thousand meters. The Quaternary stratovolcanoes of Ecuador belong to the northern volcanic zone of the Andes, extending from 5°N to 2°S (Thorpe et al., 1982).

The Chachimbiro geothermal area is characterized by persistent volcanic activity that began during the Pleistocene. The important volcanic complex of Huanguillaro (Fig. 1b) comprises a number of volcanic vents, such as Cotacachi, Pilavo, Yanahurcu de Piñán, and several acid domes. Radiometric dating of a pyroclastic flow related to the emplacement of one of these domes indicates an age younger than 8000 years (Aguilera, 1998). The volcanic products are highly differentiated, ranging from andesites to rhyodacites with a large volume of pyroclastic deposits, representing fundamental indicators of the presence, size, and location of a potential hydrothermal system (see Wohletz and Heiken, 1992, for discussion).

Two main tectonic trends have been recognized in the area, one longitudinal and parallel to the dominant direction of the Andean Range (NE-SW), and the other transversal, striking WNW-ESE.

3. Field work and laboratory analyses

A total of 20 water samples (17 for chemical and water isotopic analyses, and three for isotopic analyses only) were collected during two field campaigns in June 1999 and July 2001 (the sampled springs are shown in Fig. 1c). Raw, filtered (0.45 μm) and filtered-acidified (with HCl 1:1) samples were collected and stored in polyethylene bottles. Outlet temperature, pH, and alkalinity (by acidimetric titration) were determined in the field.

Water samples collected in 1999 were analysed for major chemical constituents, some trace elements, $\delta^{18}O$ and δD values of water, and tritium activity. All water samples collected in 2001 were analysed for chemistry, $\delta^{18}O$ and δD values of water, tritium, $\delta^{13}C$ of total dissolved carbonate, and $\delta^{34}S$ and $\delta^{18}O$ of dissolved SO_4. Isotope determinations were performed following standard procedures, and chemical analyses were carried out as follows:

- Li, Na, K, Mg, and Ca by atomic absorption spectrophotometry and/or atomic emission spectrophotometry;
- Cl, SO4, and NO_3 by ion chromatography;
- B, SiO2 and NH_4 by visible spectrophotometry.

As no fumaroles and steam vents are known to occur in the study area, three samples of bubbling gases from thermal springs were collected during the 2001 survey. Two (samples 101 and 103) are characterized by a very low gas/water ratio while the third (sample 110) has a higher gas/water ratio despite being located at some distance from the Chachimbiro geothermal area (Fig. 1).

The gas samples were analysed by gas-chromatography for CO_2, H_2S, H_2, N_2, CH_4, CO, O_2 and Ar, and by mass-spectrometry for He, Ne, Ar, and He and Ne isotopes.

All geochemical and isotope data used in this paper are reported in Tables 1 and 2.

4. Water chemistry

The chemistry of the spring waters sampled in the Chachimbiro area was initially investigated on the basis of relative Cl, SO_4, and HCO_3 concentrations (Fig. 2A) and relative Na + K, Mg, and Ca concentrations (Fig. 2B). Both triangular diagrams present concentrations by weight.

In Fig. 2A all the water samples have very low SO_4 and plot close to the Cl–HCO_3 side along an alignment connecting a Cl-rich end member, represented by the thermal waters, and an HCO_3-rich end member, including the cold shallow groundwaters. The water samples located between these two end members are likely to be mixtures (see below). Absence of shallow oxidation of H_2S is indicated by the near lack of SO_4, suggesting that shallow zones of upflow and boiling are not evident in the area.

A similar spread of points is recognizable in Fig. 2B, although sample compositions are more scattered than in Fig. 2A.

Not surprisingly, the Cl-rich thermal waters show high relative concentrations of alkalis, whereas Ca is the prevailing cation in the HCO_3-rich cold waters, which also exhibit significant concentrations of Mg, Na, and K.

Mixing between the Na–Cl thermal end member and Ca–HCO_3 shallow groundwaters is confirmed by plots of distinct chemical constituents against Cl, chosen as the conservative constituent of reference (Fig. 3). The mixing trend is clearly recognisable in the diagrams in which the mobile constituents B and Li are plotted against Cl, as well as in the Na–Cl plot, since Na is the major component of thermal waters and mixtures. The samples are more scattered in the K–Cl diagram, probably as a result of partial re-equilibration of K at the decreasing temperatures encountered by the thermal waters during their ascent to the surface. In an SiO_2–Cl plot (not shown), the points are even more scattered than in the K–Cl plot, because of the fairly rapid re-equilibration of the ascending and cooling waters.

Water sample compositions are more scattered in the plots of Mg, Ca, and HCO_3 versus Cl. Six samples, in particular (7, 10, A, B, H, J; Table 1), are characterized by high concentrations of Mg, HCO_3, and (except for samples A and H) of Ca. This is likely a result of the occurrence, to a degree much greater than in other waters, of rock dissolution driven by conversion of dissolved CO_2 to HCO_3^- ion. Samples A and W have, instead, unusually low Ca concentrations that are probably caused by precipitation of calcite. With the exception of the samples affected by secondary processes, the mixing trend between the Na–Cl thermal end member and the Ca–HCO_3 cold end member can, however, also be recognized in these plots.

Table 1
Chemical and isotopic composition of water from the Chachimbiro thermal area

Sample	Label	Type[a]	Date	Elevation (m asl)	t °C	pH[b]	HCO_3 (mg/L)	Ca (mg/L)	Mg (mg/L)	Na (mg/L)	K (mg/L)	Cl (mg/L)	SO_4 (mg/L)	B (mg/L)	NH_4 (mg/L)	SiO_2 (mg/L)	Li (mg/L)	NO_3 (mg/L)	$\delta^{18}O$‰ V-SMOW	$\delta^{2}H$‰ V-SMOW	^{3}H TU
101[c]	1	s	7/24/2001	2600	58.3	6.21	682	80.9	49.4	1186	141	1855	34.2	44.7	5.60	217	5.14	<1	−7.66	−69.3	0.52
102	2	s	7/24/2001	2620	53.4	6.37	616	87.5	44.8	1016	125	1601	31.9	38.4	4.70	212	4.43	<1	−7.93	−69.2	0.7
103[d]	3	s	7/25/2001	2580	47.2	6.23	861	102	54.9	1329	117	2060	29.4	52.6	7.35	183	5.48	<1	−6.87	−66.3	0.67
104	4	r	7/25/2001	2570	24.8	7.31	147	49.3	23.4	132	11.1	268	35.6	4.60	0.02	92.0	0.17	9.59	−9.00	−66.6	1.92
105	5	s	7/25/2001	2560	54.4	6.70	670	86.9	48.9	1156	145	1810	36.2	42.8	3.30	216	5.05	5.71	−7.53	−68.2	0.29
106	S1	p	7/25/2001	3950	16.7	–	–	–	–	–	–	–	–	–	–	–	–	–	−7.02	−61.6	2.01
107	S2	p	7/25/2001	3920	17.6	–	–	–	–	–	–	–	–	–	–	–	–	–	−7.30	−66.8	2.23
108	S3	r	7/25/2001	3820	6.7	–	–	–	–	–	–	–	–	–	–	–	–	–	−11.56	−82.7	2.16
109	6	r	7/26/2001	2760	10.9	7.76	156	21.8	11.9	17.4	3.45	16.8	3.28	0.36	0.03	61.0	0.04	<1	−11.78	−83.5	1.47
110	7	s	7/26/2001	2760	42.2	6.46	1737	237	139	660	63.6	884	10.8	26.4	2.95	185	2.41	<1	−8.91	−71.6	0.16
111	8	r	7/27/2001	2820	14.1	8.18	58.3	7.41	2.73	6.41	2.12	0.31	0.51	<0.03	0.01	64.0	0.01	<1	−11.19	−78.6	0.69
112	9	s	7/27/2001	3000	17.2	5.96	203	31.6	11.9	15.8	3.15	0.71	2.90	<0.03	0.01	104	0.01	<1	−10.89	−76.6	1.32
113	10	s	7/27/2001	2850	29.9	6.17	1035	221	96.6	440	58.1	784	44.3	17.0	1.69	144	1.90	6.51	−9.66	−73.7	0.7
105	11	s	6/11/1999	2560	59.1	6.25	693	91.0	48.0	1112	139	1655	35.2	40.5	6.00	124	–	–	−7.93	−70.24	0.68
M8	12	r	6/14/1999	2550	23.7	7.74	479	70.5	52.8	677	60.8	988	28.3	24.7	0.76	135	–	–	−8.77	−69.23	1.21
101	13	s	6/15/1999	2600	58.6	6.34	680	92.5	48.8	1195	141	1791	28.5	45.1	7.00	120	–	–	−7.69	−69.48	0.6
102	14	s	6/15/1999	2620	54.9	7.00	614	84.5	44.0	1036	126	1565	36.0	38.4	5.90	124	–	–	−8.2	−69.98	0.94
M11	15	r	6/15/1999	2520	21.5	8.12	394	71.0	36.0	592	50.4	887	23.0	22.7	9.50	122	–	–	−9.03	−69.86	1.01
103	16	s	6/15/1999	2580	46.9	6.19	833	107	50.0	1347	121	1971	29.6	51.4	0.30	158	–	–	−7.01	−67.09	0.51
M13	17	s	6/15/1999	2530	21.7	7.52	142	62.0	9.12	56	7.20	146	14.2	2.24	<0.1	93	–	–	−9.4	−67.06	2.06

Table 1 (*Continued*)

Sample	Label	Type[a]	Date	Elevation (m asl)	t °C	pH[b]	HCO_3 (mg/L)	Ca (mg/L)	Mg (mg/L)	Na (mg/L)	K (mg/L)	Cl (mg/L)	SO_4 (mg/L)	B (mg/L)	NH_4 (mg/L)	SiO_2 (mg/L)	Li (mg/L)	NO_3 (mg/L)	δ^{18}O‰ V-SMOW	δ^{2}H‰ V-SMOW	^{3}H TU
EUI_01	A	n.g.l.	12/4/1987	2740	41.6	7.1	1253	9.2	123	719	64	646	10.7	25.6	0.1	141	–	–	−9.23	−72.1	0.3
EUI_01	B	n.g.l.	7/11/1990	2740	41	6.7	1276	248	145	665	63.2	679	9.9	–	–	168	–	–	−9.3	−72.9	–
EUI_02	C	n.g.l.	12/5/1987	2560	46.2	6.7	716	94.8	47.2	1350	135	2040	30	49.7	7.1	182	–	–	−7.11	−69	0.9
EUI_03	D	n.g.l.	12/6/1987	2590	45.6	7.5	506	84.9	44.4	1230	135	1860	32	44.3	3	204	–	–	−7.38	−68.5	0.4
EUI_03a	E	n.g.l.	7/10/1990	2618	58.1	6.3	661	76.7	47.7	1250	155	2040	30.9	–	–	200	–	–	−7.6	−70.2	–
EUI_04	F	n.g.l.	12/7/1987	2530	31.7	6.8	1235	86.0	82.3	1660	67	2250	10.1	61.4	0.1	123	–	–	−6.03	−64	0.3
EUI_05	G	n.g.l.	12/6/1987	2200	23.1	7.2	397	47.2	37.3	104	10.9	94.5	4.5	2.2	0.1	97.1	–	–	−9.87	−73.6	0.3
EUI_06	H	n.g.l.	12/6/1987	2155	30.7	7.3	1016	69.5	135	387	34.7	618	11.5	14.7	0.1	129	–	–	−9.42	−70.3	0.3
EUI_06	J	n.g.l.	7/11/1990	2155	30.6	6.8	1013	162	149	351	28	597	9.9	–	–	98	–	–	−9.5	−69.1	–
EUI_07	W	n.g.l.	12/7/1987	2570	40.4	7.2	1090	41.0	63.9	1420	62.5	1890	11.7	50.4	0.1	158	–	–	−6.98	−67.5	0
EUI_11	L	n.g.l.	12/9/1987	3570	9.1	7.0	37	2.8	0.9	6.0	2.7	0.8	1.5	0	0.1	41.2	–	–	−11.93	−65.6	3.3
EUI_12	M	n.g.l.	12/10/1987	2730	21.6	6.8	250	40.4	15.4	33.2	6.4	1.6	1.5	0.1	0.1	121	–	–	−10.82	−76.2	1.1
EUI_31	N	n.g.l.	7/11/1990	2190	28.8	6.4	771	61.6	40.9	326	13.4	404	2.4	–	–	114	–	–	−10	−72.7	–
EUI_32	O	n.g.l.	7/12/1990	3618	7	–	139	18.8	7.4	9.3	2.7	0.2	0.6	–	–	61	–	–	−12.7	−90.5	–
EUI_33	P	n.g.l.	7/12/1990	3610	7	–	93	13.1	6.3	5.9	2.1	0.2	0.9	–	–	48	–	–	−13.2	−93.1	–
EUI_34	Q	n.g.l.	7/13/1990	3305	17	–	141	21.3	6.4	14.6	2.9	0.2	11.1	–	–	117	–	–	−12	−82.5	–

n.g.l.: data taken from literature; type of samples not defined.

[a] s: spring; r: river; p: pond.

[b] the pH data from this study were measured directly in the field.

[c] δ^{13}C TDIC (total dissolved inorganic carbon) = −2.16‰ vs. PDB (Pee Dee Belemnite); δ^{34}S SO_4 = 13.66‰ vs. CDT (Canyon Diablo Troilite); δ^{18}O SO_4 = 12.52‰ vs. V-SMOW (Vienna-Standard Mean Ocean Water).

[d] δ^{13}C TDIC = −1.93‰ vs. PDB.

Table 2
Chemical composition of free gases in Chachimbiro and Timbuyacu thermal springs (a); He and Ne chemical and isotope composition (b)

(a)

Sample	Location	Date	CO_2 μmol/mol	H_2S μmol/mol	N_2 μmol/mol	O_2 μmol/mol	Ar μmol/mol	H_2 μmol/mol	CH_4 μmol/mol	CO μmol/mol
101[a]	Chachimbiro	7/24/2001	974654	0	16414	8459	322	0.50	141	9.3
103[b]	Chachimbiro	7/25/2001	972700	0	17350	9287	469	1.33	189	3.2
110	Timbuyacu	7/26/2001	976250	0	15592	7695	364	0.81	991	5.4

(b)

Sample	Location	Date	R/Ra	Standard deviation	(R/Ra)c	He/Ne	He (μmol/mol)	Ne (μmol/mol)
101	Chachimbiro	7/24/2001	1.02	0.16	1.03	0.94	0.19	0.2
103	Chachimbiro	7/25/2001	1.34	0.04	2.89	0.34	0.43	1.3
110	Chachimbiro	7/26/2001	1.48	0.12	1.76	0.77	0.28	0.4
air			1	–	0.32	0.29	5.24	18.2
asw			1	–	0.28	–	0.05	0.2

(R/Ra)c: air correction using the formula $(R/Ra)c = [(R/Ra) \times x - 1]/(x - 1)$ where $x = (He/Ne)_{meas}/(He/Ne)_{air/asw}$.
[a] $\delta^{13}C\ CO_2 = -4.56‰$ vs. PDB.
[b] $\delta^{13}C\ CO_2 = -4.76‰$ vs. PDB.

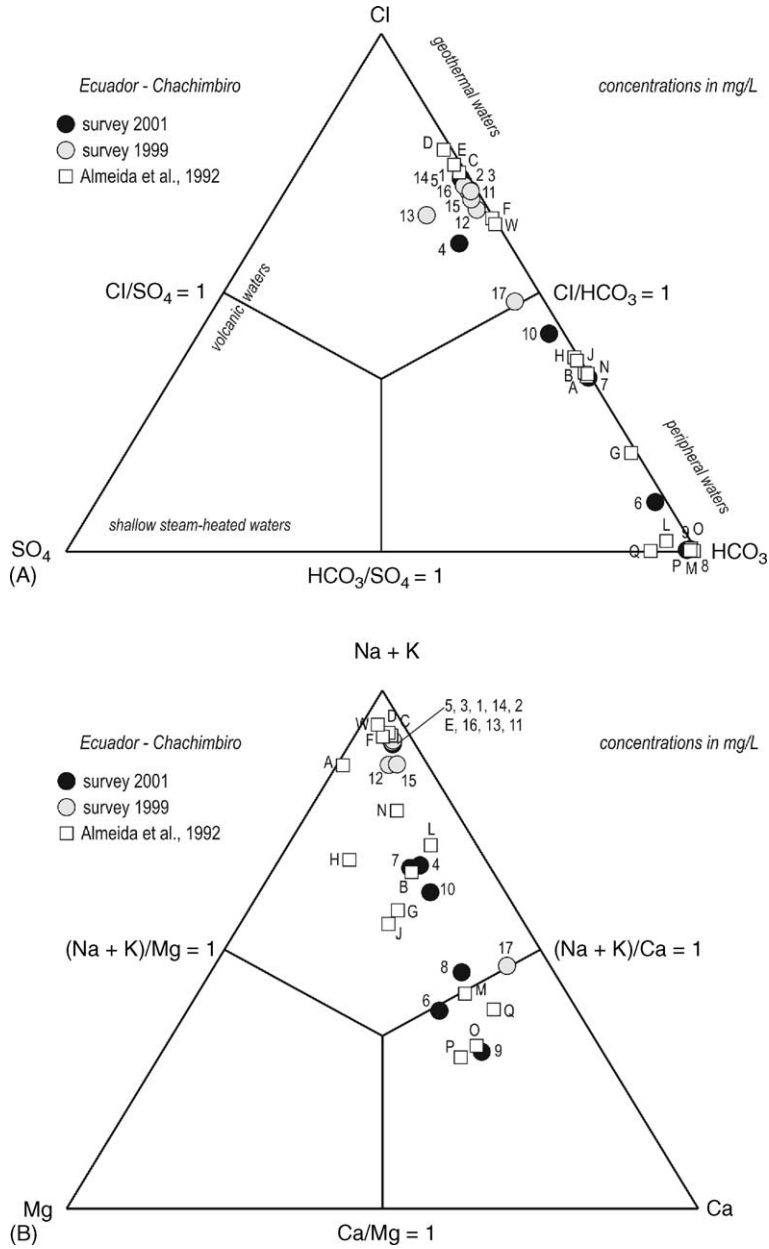

Fig. 2. (A) Relative concentrations of Cl, SO_4, and HCO_3 and (B) relative concentrations of Na + K, Mg, and Ca (all in equivalent units) for the Chachimbiro discharges. See Table 1 for details of samples and sampling locations.

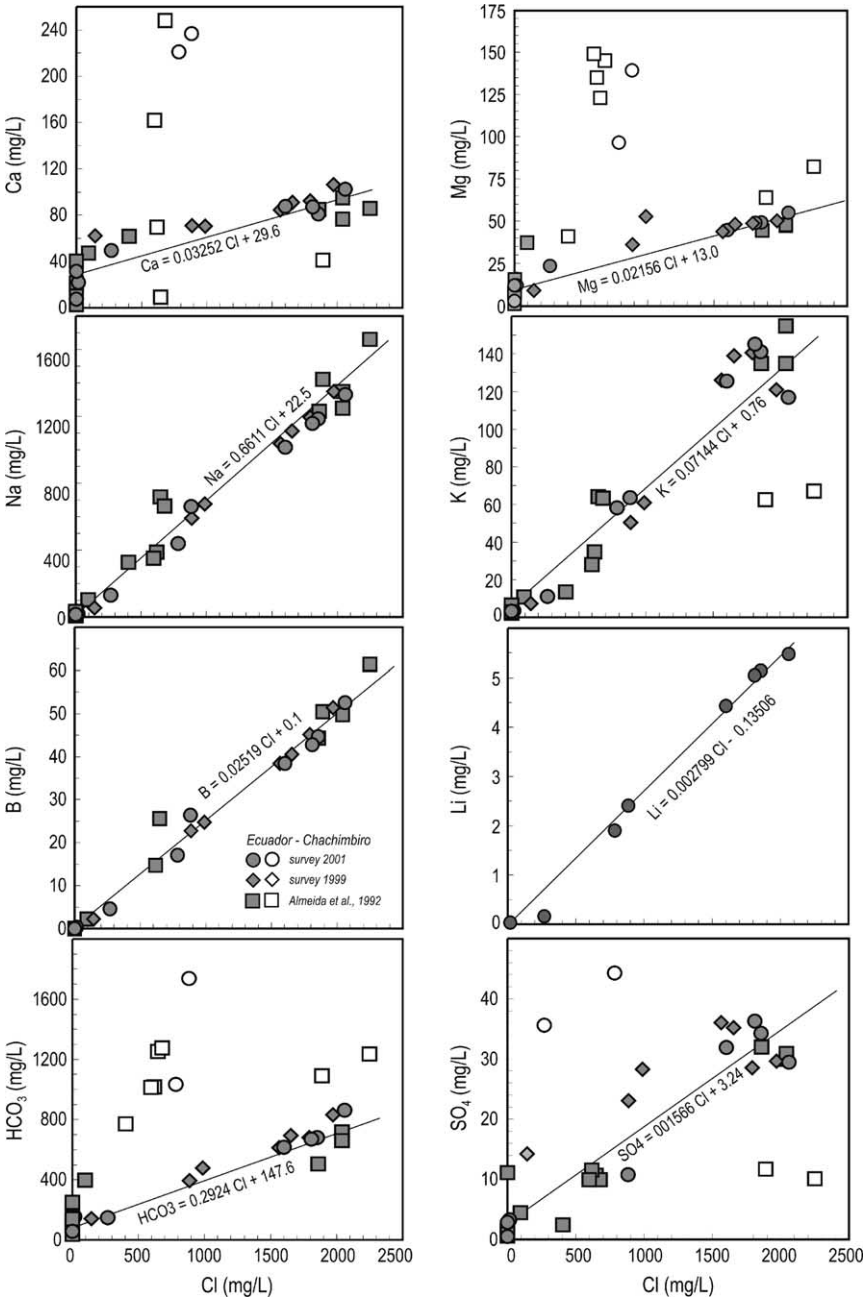

Fig. 3. Plots of Ca, HCO_3, Na, K, B and SO_4 against Cl for the springs in the Chachimbiro geothermal area. Also shown is the mixing line of the Cl-rich thermal end member with the Cl-poor cold end member. The open and closed symbols indicate that the springs have been excluded or included, respectively, when constraining the mixing trend in the linear regression.

5. Chemical geothermometers based on aqueous solutes

The Na–K–$Mg^{1/2}$ triangular diagram of Giggenbach (1988) is a powerful and widely used geothermometer. The original Giggenbach diagram has been slightly modified here (Fig. 4) by constructing the full equilibrium line on the basis of the K–Mg geothermometer of Giggenbach (1988) and the Na–K geothermometer of Fournier (1979), because, in our opinion, the latter is more applicable here than the Giggenbach equation. There are two reasons for this: first, it was thoroughly calibrated on the basis of equilibrated water discharges from deep geothermal wells and oil-field brines and, second, it closely approaches the Na–K ratio constrained by the albite/K-feldspar/aqueous solution equilibrium, according to the thermodynamic data of Johnson et al. (1992) (see also Pang, 1992, and references therein for more discussions). In Fig. 4 all the Chachimbiro thermal spring samples plot in the field of immature waters, because of their relatively high Mg concentrations, which result in K–Mg temperatures (105–115 °C for the most saline waters) that are far lower than the maximum estimated Na–K temperature of 235 °C. The quartz geothermometer of Fournier and Potter (1982) gives a maximum equilibrium temperature of 189 °C for the most saline Chachimbiro thermal springs, in contrast with both the Na–K and K–Mg geothermometers. The estimated quartz temperatures, however, have to be considered as the lowest estimates. The silica versus temperature diagram (Fig. 5) shows, in fact, that thermal waters attain

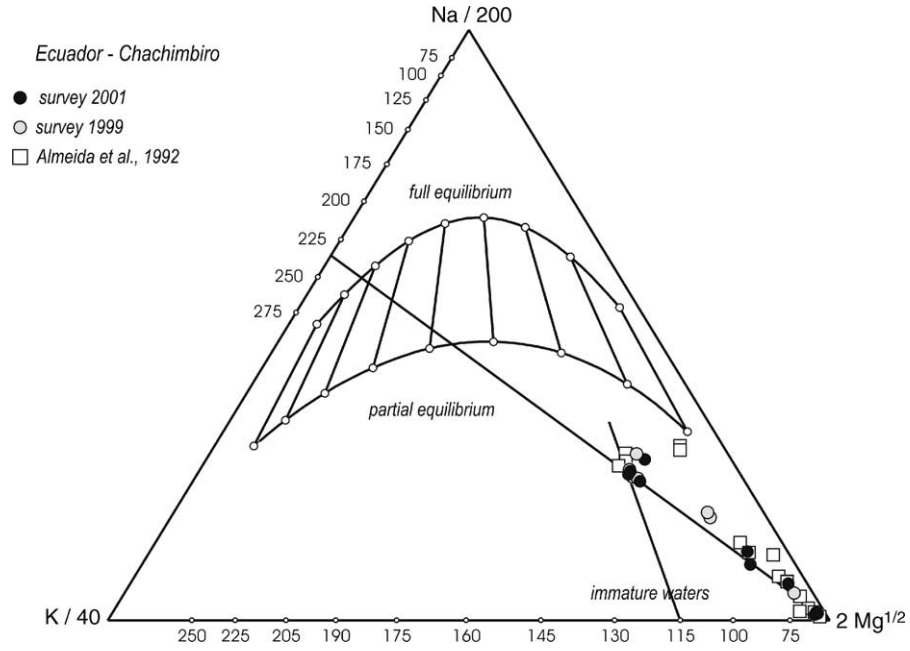

Fig. 4. Na–K–$Mg^{1/2}$ triangular diagram for the Chachimbiro discharges. The plot of Giggenbach (1988) was modified by drawing the full equilibrium line based on the K–Mg geothermometer of Giggenbach (1988) and the Na–K geothermometer of Fournier (1979).

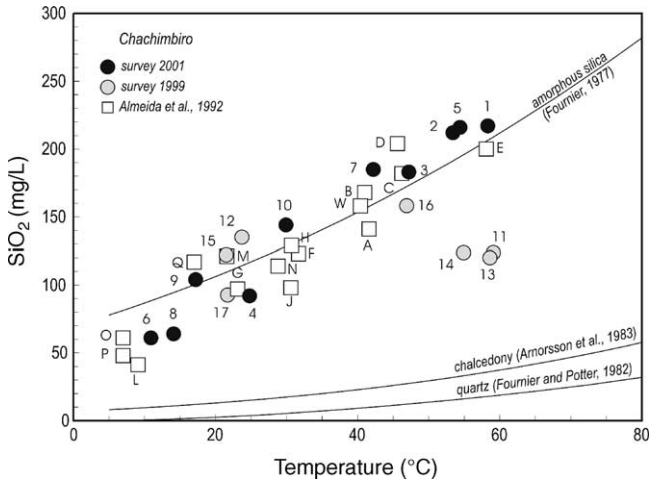

Fig. 5. Silica vs. temperature diagram, showing the saturation lines with respect to relevant silica polymorphs. See Table 1 for details of samples and sampling locations (Arnórsson et al., 1983; Almeida et al., 1992; Fournier, 1977; Fournier and Potter, 1982).

saturation with amorphous silica and likely precipitate this phase during their ascent to the surface.

6. Composition of the parent geothermal water

To obtain the composition of the parent undiluted geothermal water, the concentrations of all dissolved constituents, apart from SiO_2 and Mg, were first regressed against Cl, excluding the samples affected by mixing and other secondary processes. The concentration of each chemical constituent in the parent geothermal water was then obtained by using the Cl concentration of the most saline sample, 2250 mg/L, in the pertinent regression equation (Table 3). The possible existence of a parent geothermal water with a Cl content higher

Table 3
Linear regression equations describing mixing of the thermal and the cold end members

$Ca = 0.03252 \times Cl + 29.6$
$Na = 0.66110 \times Cl + 22.5$
$K = 0.07144 \times Cl + 0.76$
$Mg = 0.02156 \times Cl + 13.0$
$HCO_3 = 0.29240 \times Cl + 147.6$
$SO_4 = 0.01566 \times Cl + 3.24$
$B = 0.02519 \times Cl + 0.1$
$Li = 0.00279 \times Cl - 0.135$
$H = 0.09935 \times Cl + 67.1$
$\delta^2H = 0.001727 \times Cl - 71.7$
$\delta^{18}O = 0.001548 \times Cl - 10.3$

Concentrations are in mg/L. Enthalpy (H) is in J/g. δ^2H and $\delta^{18}O$ values in % vs. V-SMOW.

than 2250 mg/L cannot, however, be ruled out. Because of probable silica loss (see above), the SiO_2 concentration of the deep-water was computed by assuming equilibrium, using a temperature of 235 °C (estimated from the Na/K geothermometer discussed above) in the quartz geothermometer equation (Fournier and Potter, 1982). We thus obtained a value of 410 mg/L. Based on the same hypothesis, the concentration of Mg in the deep water was calculated by inserting the deep water K concentration, 162 mg/L, and the estimated temperature of 235 °C in the K–Mg geothermometer function to calculate a deep water Mg concentration of 0.13 mg/L.

Assuming that Mg is acquired downstream of the deep reservoir through rock dissolution driven by CO_2 conversion to HCO_3^- ion, each mole of acquired Mg^{2+} is accompanied by two moles of acquired HCO_3^-, due to the electroneutrality constraint. The increase in HCO_3 concentration, Δ_{HCO_3} (mg/L), was therefore obtained by means of the following relationship:

$$\Delta_{HCO_3} = 2\left(\frac{\Delta_{Mg}}{MW_{Mg}}\right) MW_{HCO_3} \quad (1)$$

where MW is molecular weight.

The restored deep water HCO_3 concentration is, therefore, 498 mg/L.

Ca is also likely acquired through the same mechanism as Mg. The Ca and HCO_3 concentrations and the P_{CO_2} initially present under reservoir conditions can be computed by using different P_{CO_2}-indicators, adopting the approach proposed by Marini et al. (1998). Relevant P_{CO_2}-indicators are the K–Ca function of Giggenbach (1988) (with P_{CO_2} in bars; concentrations in mg/L):

$$\log P_{CO_2} = \log\left(\frac{K^2}{Ca}\right) - 3.0 \quad (2)$$

and the K–Ca, Ca–Mg, and HCO_3 functions of Chiodini et al. (1991) (with P_{CO_2} in bars; T in K; concentrations in mol/kg):

$$\log P_{CO_2} = 1.106 \log HCO_3 + 5.773 + 0.541 \log \Sigma eq - 3565.3/T \quad (3)$$

$$\log P_{CO_2} = 2.179 \log K^2/Ca - 14.405 - 1.275 \log \Sigma eq + 3451/T \quad (4)$$

$$\log P_{CO_2} = -1.341 \log Ca/Mg + 9.772 + 0.523 \log \Sigma eq - 3485.3/T \quad (5)$$

where Σeq is total ionic salinity in eq/kg.

Direct application of these P_{CO_2}-indicators to the parent geothermal water results in very different P_{CO_2} values. Assuming that the reason for these discrepancies is Ca acquisition through rock dissolution driven by CO_2 conversion to HCO_3^- ion, the increases in Ca and HCO_3 concentrations are linked by an equation similar to Eq. (1). Calcium and HCO_3 concentrations were therefore computed for variable increases in Ca concentration (ΔCa) and plugged into the relevant -indicators (Eqs. (2)–(5)). The P_{CO_2} values obtained are plotted versus ΔCa in Fig. 6. This plot shows that the HCO_3 function is almost flat whereas the other P_{CO_2}-indicators curve strongly, converging towards the HCO_3 function for P_{CO_2} of ~5.1 bar and ΔCa of 95.6 ± 5.5 mg/L. Consequently, the restored Ca and HCO_3 concentrations (i.e.

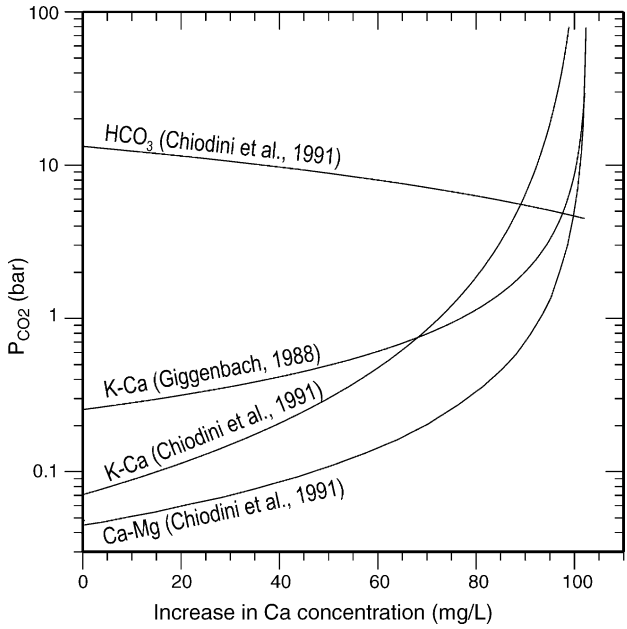

Fig. 6. Plot of P_{CO_2} vs. the increase in Ca concentration caused by rock dissolution driven by CO_2 conversion to HCO_3^- for the Chachimbiro parent geothermal water. The P_{CO_2} was computed using different P_{CO_2}-indicators proposed by Giggenbach (1988) and Chiodini et al. (1991).

before Ca leaching sets in) are 7.4 and 207 mg/L, respectively. The equilibrium P_{CO_2} of 5.1 bar corresponds to a total carbon content of 3230 mg/L as HCO_3.

Table 4 shows a comparison between geothermometric temperatures for the parent geothermal liquid and some spring samples.

The pH of the parent geothermal water was then calculated on the basis of the equilibrium P_{CO_2} and the concentration of the HCO_3^- ion, using the computer code EQ3NR, version 7.2 (Wolery, 1992). This program takes into account the dissociation of relevant weak acids and main aqueous complexes and computes the activity coefficients of ionic species by means of the modified Debye–Hückel equation. The resulting calculated pH of the parent geothermal water is 6.10. Its complete composition is given in Table 5.

7. Saturation state of the parent geothermal water with respect to relevant minerals

As shown by Giggenbach (1984), in many geothermal systems located along convergent plate boundaries, the P_{CO_2} values of the deep geothermal water are fixed, at given temperatures, by the full equilibrium assemblage comprising calcite, a Ca–Al silicate, K-feldspar, K-mica and chalcedony. Consequently, the P_{CO_2} can be obtained from the mineral-solution

Table 4
Geothermometric temperatures (in °C) for the parent geothermal liquid and the Na–Cl waters with a contribution of parent geothermal liquid higher than 1/3

Sample	Label	Quartz[a]	Chalcedony[b]	Amorphous silica[b]	Na–K[c]	K–Mg[d]
Parent geothermal liquid		225	210	98	223	228
101	1	186	165	62	232	116
102	2	185	163	60	235	113
103	3	175	152	51	206	109
105	5	186	165	61	237	117
110	7	175	153	51	214	80
113	10	159	134	36	242	82
M7	11	150	124	28	237	116
M8	12	155	130	33	208	91
M9	13	148	122	26	232	116
M10	14	150	124	28	234	114
M11	15	149	123	27	203	91
M12	16	165	141	42	208	111
EUI_02	C	174	152	50	217	115
EUI_03	D	182	160	58	225	116
EUI_03a	E	181	159	56	236	119
EUI_04	F	149	124	28	150	88
EUI_07	W	165	141	42	156	89

[a] Fournier and Potter (1982).
[b] Fournier (1973).
[c] Fournier (1979).
[d] Giggenbach (1988).

equilibrium temperature using the following equation (T in °K, P_{CO_2} in bar):

$$\log P_{CO_2} = 0.0168(T - 273.15) - 3.78 \quad (6)$$

The P_{CO_2} value estimated for the Chachimbiro parent water, 5.1 bar, is much higher than that fixed by coexistence of calcite and a Ca–Al silicate at the equilibrium temperature of 235 °C, i.e. 1.5 bar. This difference suggests that Ca–Al silicates are unstable under the P_{CO_2} and temperature conditions prevailing in the Chachimbiro geothermal reservoir. High-P_{CO_2} geothermal systems are an unusual occurrence along convergent plate margins, but they do exist, as documented, for instance, at Broadlands, New Zealand (Mahon and Finlayson, 1972).

In order to investigate this matter further, the saturation indices with respect to a number of hydrothermal minerals potentially present in the Chachimbiro geothermal reservoir were calculated for the parent geothermal water at a temperature of 235 °C by means of the EQ3NR code. Since aluminum was not measured in the collected samples, the Al concentration in the parent geothermal water was assumed to be fixed by saturation with K-feldspar (Pang and Reed, 1998). This mineral was selected because, with the exception of strongly acidic environments (which do not occur at Chachimbiro), it is a widespread hydrothermal mineral in the 150–350 °C range (e.g. Henley and Ellis, 1983), and usually occurs as a pure phase. The parent geothermal water of Chachimbiro is close to saturation with chalcedony and quartz, albite, muscovite, calcite, and Na-, Ca-, and Mg-montmorillonites, whereas it

Table 5
Calculated chemical and isotopic composition and saturation indices with respect to relevant minerals for the geothermal liquid possibly present in the Chamchimbiro geothermal reservoir

Component (species)	Concentration (mg/kg)	Minerals	log (Q/K)	Affinity (kcal/mol)
Na	1510	Albite	−0.102	−0.231
K	162	Anhydrite	−0.805	−1.834
Mg	0.19	Calcite	−0.086	−0.197
Ca	7.5	Chalcedony	−0.073	−0.167
Cl	2250	Clinochlore-14A	−3.018	−6.880
SO_4	38.5	Clinozoisite	−2.392	−5.452
HCO_3	207	K-Feldspar	−0.061	−0.139
C_{TOT} (as HCO_3)	3300	Laumontite	−1.257	−2.866
SiO_2	357	Montmorillonite-Ca	−0.079	−0.180
B	56.8	Montmorillonite-K	−0.517	−1.180
Al	0.181	Montmorillonite-Mg	−0.163	−0.372
		Montmorillonite-Na	−0.361	−0.823
Other parameters		Muscovite	0	0
pH	6.14	Paragonite	−0.701	−1.597
P_{CO_2} (bar)	5.0	Prehnite	−1.719	−3.919
δ^2H (vs. V-SMOW)	−67.8	Quartz	0.089	0.203
$\delta^{18}O$ (vs. V-SMOW)	−6.82	Saponite-Ca	0.123	0.280
		Saponite-K	−0.535	−1.219
		Saponite-Mg	−0.003	−0.006
		Saponite-Na	−0.200	−0.457
		Wairakite	−1.600	−3.646

is undersaturated with respect to clinochlore and several Ca–Al silicates, such as clinozoisite, laumontite, prehnite, and wairakite (Table 5). These data confirm that, under these comparatively high P_{CO_2} conditions, calcite is the stable mineral governing dissolved Ca activity rather than the Ca–Al silicates, and that the montmorillonites constrain dissolved Mg activity instead of clinochlore (chlorites).

8. Geochemistry of free gases

The gas samples collected in the Chachimbiro geothermal area are virtually free of sulfur species and mainly consist of CO_2, which accounts for 97.2–97.6 mol % of the total gas (Table 2). Nitrogen represents the second major constituent of the gas mixtures, with concentrations up to 1.6 mol%. Entry of air and air-saturated waters into the natural system has a significant effect on the bulk gas composition, as indicated by the high O_2 and Ar contents compared to those of N_2, and by the lack of H_2S. In particular, the N_2/Ar and O_2/Ar ratios of 51–37 and 26–20 for the gas from sites 101 and 103, respectively (Table 2), are very close to the values expected for air-saturated groundwater at 55 °C, i.e. 43 and 21, respectively (gas solubility data from Wilhelm et al., 1977). Since atmospheric components are controlled by water–air equilibrium, great care must be taken when attempting a quantitative evaluation of deep equilibrium conditions from the starting-point of these

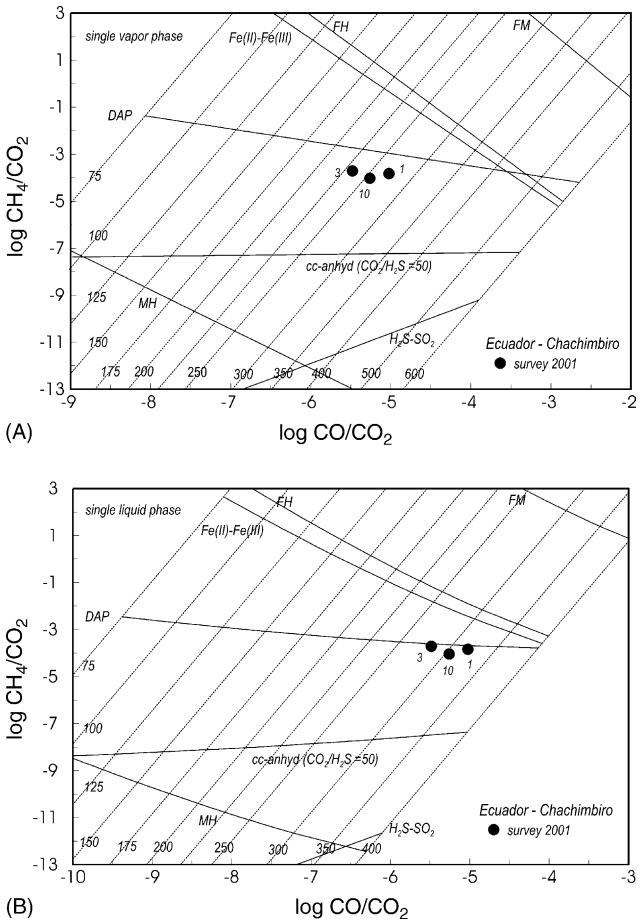

Fig. 7. Equilibrium log (CH_4/CO_2) and log (CO/CO_2) molar ratios under temperatures and redox conditions fixed by different buffers in (A) a single vapor phase and (B) a single liquid phase. Also shown are the analytical molar ratios of Chachimbiro discharges. Buffers of fO_2 are as follows: DAP: D'Amore and Panichi (1980); Fe(II)–Fe(III): rock-dominated hydrothermal buffer; H_2S–SO_2: gas-dominated magmatic buffer; FM: fayalite–magnetite; FH: fayalite–hematite; MH: magnetite–hematite; Giggenbach (1987); cc-anhyd: calcite-anhydrite; Giggenbach (1993).

gas analytical data. The hydrogen contents are probably lower than the CO concentrations because of the occurrence of H_2-consuming secondary processes.

The ratios between C species are, however, close to the values expected for equilibrium, under the redox conditions described by the f_{O_2} buffer of D'Amore and Panichi (1980), at temperatures of either $\sim 260 \pm 25\,^{\circ}C$ in a single vapour phase or $\sim 310 \pm 25\,^{\circ}C$ in a single liquid phase (Fig. 7). Despite the uncertainties that derive from the secondary processes affecting these thermal waters during their ascent towards the surface, these temperatures could be present at the root of the Chachimbiro geothermal system.

The measured He isotope ratios range between 1.02 and 1.48 Ra (where Ra stands for the $^{3}He/^{4}He$ of air). These He isotope ratios, when corrected for air addition, according to Craig et al. (1978), range between 1.03 and 2.89 Ra (Table 2). Although the latter value is affected by a significant uncertainty related to the correction, it does suggest an input of mantle-derived He into the Chachimbiro geothermal system.

9. Isotope composition of water

In the classic $\delta^{2}H$ versus $\delta^{18}O$ diagram (Fig. 8), local Cl-poor groundwaters plot close to the Global Meteoric Water Line, whereas the thermal waters again show an alignment

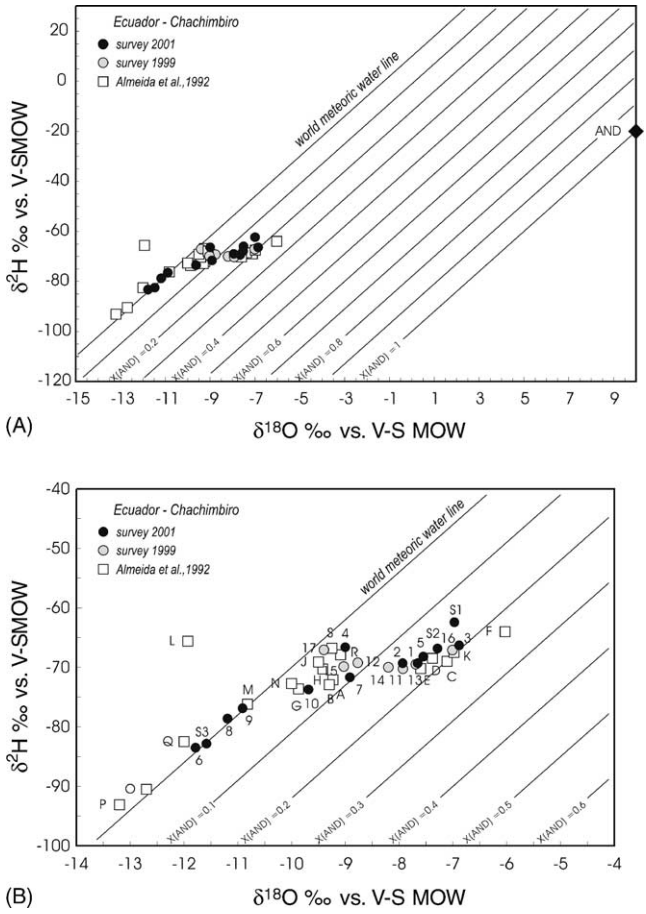

Fig. 8. $\delta^{2}H$ vs. $\delta^{18}O$ diagram, showing the isotopic composition of waters discharging in the Chachimbiro area. Also shown is the worldwide meteoric water-line, the average isotope composition of arc-type magmatic water (Giggenbach, 1992), and the mixing line between arc-type magmatic water and local groundwaters of meteoric origin. AND: andesite. See Table 1 for details of samples and sampling locations.

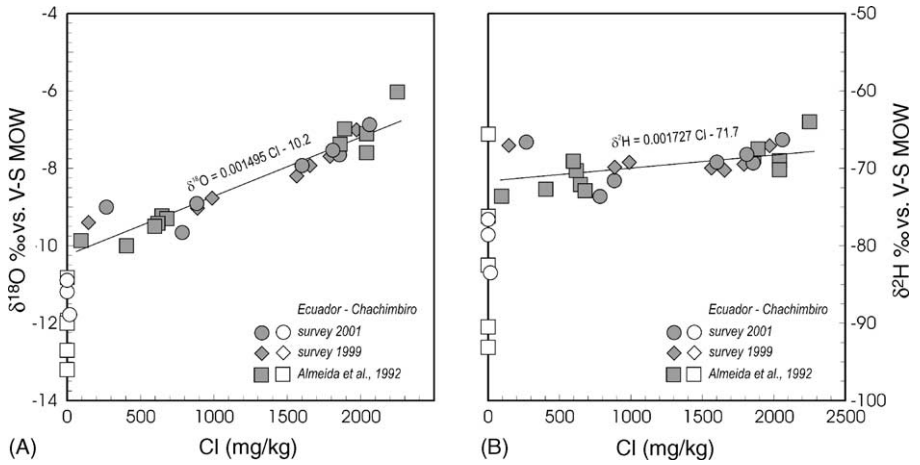

Fig. 9. Plots of (A) $\delta^{18}O$ values vs. Cl and (B) $\delta^{2}H$ values vs. Cl for the springs of the Chachimbiro area. Also shown is the mixing line of the Cl-rich thermal end member with the Cl-poor local groundwaters. The open and closed symbols refer to the springs either excluded or included in the linear regression to define the mixing trend.

resulting from the dilution affecting the Chachimbiro geothermal water. Dilution is confirmed by the plots of $\delta^{18}O$ versus Cl (Fig. 9A) and $\delta^{2}H$ versus Cl (Fig. 9B). The linear regression equations fitting the thermal water trend, in these two Cl-plots, indicate $\delta^{2}H$ and $\delta^{18}O$ values of -71.9 and -10.3‰ for the local groundwaters involved in the mixing process, and –67.7 and –6.82‰ for the parent geothermal water.

In Fig. 8, extrapolation of the thermal water trend towards higher $\delta^{2}H$ and $\delta^{18}O$ values does not pass through the point representative of arc-type magmatic water, i.e. $\delta^{2}H = -20$‰ and $\delta^{18}O = +10$‰ (Giggenbach, 1992). This suggests that an input of arc-type magmatic water at the roots of the Chachimbiro geothermal system is not the only process controlling the oxygen isotope shift of these geothermal waters, but it is most likely coupled with significant water/rock exchange of oxygen isotopes. The effects of these two processes were quantified by projecting, at constant $\delta^{2}H$, the point representative of the parent geothermal water onto the mixing line between arc-type magmatic water and local groundwaters of meteoric origin. It turns out that the isotopic composition of the parent geothermal water is compatible with a mixing of 8% arc-type magmatic water and 92% local groundwater of meteoric origin, coupled with a water/rock ^{18}O shift of 1.9‰ units. Since we used a rather high $\delta^{18}O$ value for the arc-type magmatic water, this ^{18}O shift is a minimum estimate, whereas this choice has little effect on the relative proportions of arc-type magmatic water and local groundwater.

In Fig. 9B, by extrapolating the thermal water trend to the average $\delta^{2}H$ value of arc-type magmatic water, we obtained a Cl concentration of ∼28,000 mg/L for the magmatic end member. This Cl content corresponds to an H_2O/Cl molar ratio close to 70, which is relatively low, but within the range found in high-temperature fumarolic discharges from convergent plate boundaries (i.e. molal H_2O/Cl of 14–5300; Symonds et al., 1994).

10. δ^{13}C values of total dissolved carbonate

Carbon isotope ratios of −2.16 and −1.93‰ PDB (Pee Dee Belemnite) were measured for the total carbonate species dissolved in samples 101 and 103 from Chachimbiro springs. Calculated δ^{13}C values for gaseous CO_2 in equilibrium with these samples are −4.29 and −4.19‰, respectively. These isotope values are close to the upper limit, but within the range usually accepted for magmatic CO_2 of −4 to −8‰ (Deines and Gold, 1973; Kyser, 1986). However, the δ^{13}C value of magmatic CO_2 can exhibit wide variations, depending on the extent of degassing and the type of gas separation, as well as melt composition and temperature (Blank and Brooker, 1994; Holloway and Blank, 1994). Along convergent plate boundaries, moreover, the magmatic source might be affected by contamination deriving from the subduction of carbonate-rich sediments, which is expected to bring about an increase in the isotope values of magmatic CO_2. All in all, the δ^{13}C values measured at Chachimbiro suggest a magmatic origin for the CO_2 of the geothermal system.

11. δ^{34}S values of dissolved sulfate

The measured δ^{34}S of dissolved SO_4 in sample 101 was +13.66‰ CDT (Canyon Diablo Troilite). This comparatively heavy isotope value is probably the result of extensive bacterial SO_4 reduction, which is very common under a variety of natural conditions and is usually described by the reaction:

$$SO_4^{2-} + 2CH_2O = 2HCO_3^- + H_2S \tag{7}$$

where CH_2O indicates the organic matter involved in the process (e.g. Berner and Berner, 1996; Marini et al., 2000). Assuming that sulfide generated by bacterial SO_4 reduction separates from the system through H_2S degassing or precipitation of either pyrite or other sulfide minerals, these separation processes can follow two limiting mechanisms, either open-system (continuous or Rayleigh) or closed-system (single-step or batch). Open-system sulfide separation brings about the following changes in the δ^{34}S value of dissolved SO_4:

$$\delta^{34}S_f = (\delta^{34}S_i + 1000)F^{\alpha-1} - 1000 \tag{8}$$

whereas closed-system sulfide separation is described by the equation:

$$\delta^{34}S_f = \delta^{34}S_i + (F-1)1000 \ln \alpha \tag{9}$$

where F is the fraction of sulfate remaining in the system, α is the H_2S–SO_4 fractionation factor, and subscripts f and i refer to the final and initial states, respectively (e.g. Ohmoto and Goldhaber, 1997). The H_2S–SO_4 kinetic fractionation factor typically varies from −15 to −60‰, depending on reaction rate, pH, temperature, and other factors. However, the equilibrium H_2S–SO_4 fractionation factor (Ohmoto and Goldhaber, 1997) is −60‰ at 59 °C, which is the maximum outlet temperature of Chachimbiro thermal springs, and −26‰ at 235 °C, the estimated equilibrium temperature of the deep geothermal reservoir.

Unfortunately, no δ^{34}S data are available for either sulfate or dissolved sulfide on Chachimbiro samples, but δ^{34}S values were determined for dissolved H_2S in two spring

samples from the Tufiño thermal area (which is located about 60 km NE of Chachimbiro): Aguas Hediondas, −1.70‰, and Aguas Negras, −3.24‰. Assuming that the average of these two values is representative of the S-isotope composition of the dissolved H_2S of Chachimbiro, a $\Delta_{H_2S-SO_4} = 1000 \ln \alpha$ of −16 (±1)‰ is obtained.

The initial (i.e. before bacterial SO_4 reduction sets in) SO_4 concentration in Chachimbiro geothermal waters can be obtained by assuming anhydrite saturation under reservoir conditions. Based on this hypothesis, an initial SO_4 concentration of 234 mg/L was computed for the parent geothermal water, using the EQ3NR code. The corresponding value of F is, therefore, 38.5/234 = 0.165. Taking $1000 \ln \alpha = -16‰$, $\delta^{34}S_i$ values of −15 and +0.3‰ are obtained, under open- and closed-system separation, respectively, for the parent geothermal water.

Despite the large uncertainties in the initial S isotope ratios, these simple calculations demonstrate that bacterial SO_4 reduction can greatly affect the isotopic composition of dissolved SO_4. Positive values such as that measured at Chachimbiro do not exclude that the S species present in the geothermal system are of magmatic provenance ($\delta^{34}S$ value close to 0‰) or derive from sulfide minerals with negative $\delta^{34}S$ values.

12. $\delta^{18}O$ values of dissolved sulfate

The $\delta^{18}O$ of dissolved sulfate was measured only for sample 101 from a Chachimbiro spring; the sample was collected in 2001, and a value of +12.5‰ obtained. An apparent equilibrium temperature close to 75 °C is inferred by coupling this value with the $\delta^{18}O$ of water, −7.66‰. It must be emphasized that this sample has 1855 mg/L Cl and can therefore be interpreted as a mixture of 82% parent geothermal water and 18% groundwater. The influence of mixing on the $\Delta^{18}O(SO_4–H_2O)$ geothermometer was investigated by McKenzie and Truesdell (1977), but, in the case of Chachimbiro, the effect of mixing cannot be evaluated because only one sample was available. The apparent equilibrium temperature could also be affected by other interfering processes, such as bacterial sulfate reduction (see above), but again no correction can be applied due to the lack of essential information.

13. Conceptual geochemical model and concluding remarks

As indicated by water isotopes, the Chachimbiro geothermal system is mainly recharged by meteoric water (92%) and secondarily by arc-type magmatic water (8%) with a relatively low H_2O/Cl molar ratio of ∼70. Although interpretation of the $\delta^{13}C$ of CO_2 and the $\delta^{34}S$ of dissolved SO_4 is somewhat ambiguous, these data are in line with a magmatic origin for the C and S species discharged by the geothermal system. CO_2 and S gases, along with H_2O, released from a degassing magma body, are therefore likely to enter the roots of the Chachimbiro geothermal system from below. This conclusion is supported by the evidence provided by He isotopes. A schematic hydrogeological cross-section of the Chachimbiro geothermal area is shown in Fig. 10.

Temperatures higher than 260 °C could be present in the deepest parts of the geothermal system, as suggested by $CO_2–CH_4–CO$ equilibria, whereas water geothermometers suggest

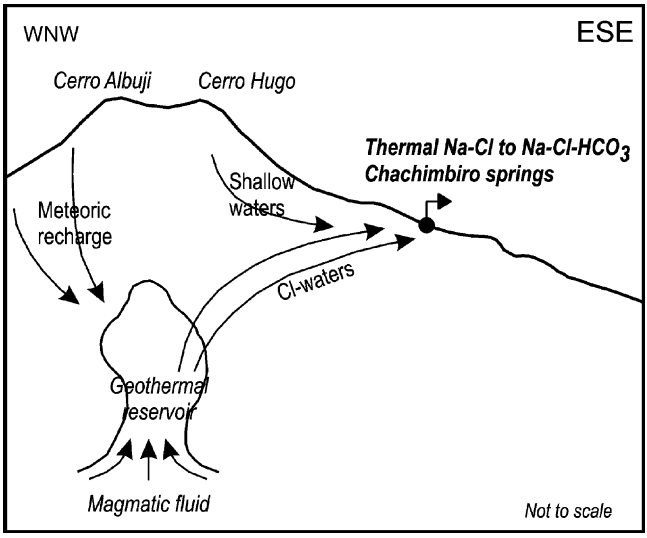

Fig. 10. Schematic hydrogeological cross-section of the Chachimbiro geothermal area.

the presence of a geothermal reservoir at ∼235 °C. The parent geothermal water has likely 2250 mg/L Cl and cools through mixing with cold waters along the upflow path from the shallow reservoir to the surface.

The P_{CO_2} of the parent geothermal water is close to 5 bars, a value that is significantly higher than 1.5 bar, which is the P_{CO_2} fixed by calcite/Ca–Al silicate coexistence at reservoir temperatures. Under the P_{CO_2} and temperature conditions that are presumably present in the Chachimbiro geothermal system, Ca–Al silicates are unstable and dissolved Ca activity is fixed by calcite saturation. These inferences are confirmed by speciation/saturation models, which indicate that the parent geothermal water of Chachimbiro is close to saturation with calcite, chalcedony and quartz, albite, muscovite, and Na-, Ca-, and Mg-montmorillonites.

The Chachimbiro area therefore appears to be very promising regarding the possible existence of a high-enthalpy geothermal reservoir that could be exploited for electric power generation and certainly deserves the highest priority of all the geothermal areas investigated so far in Ecuador. It should, however, be pointed out that only geochemical and isotope data are currently available for this area, with little or no important data available of a volcanological, hydrogeological, and geophysical nature.

Acknowledgements

This paper was based on the results of the IAEA technical cooperation project for Ecuador-ECU/8/019. The financial and technical support of the IAEA and the Ecuadorian government is gratefully acknowledged. The authors would like to thank Halldór Ármannsson and Bruce Christenson for reviewing the manuscript. They are grateful to

Alfred Truesdell, one of the Guest Editors of this issue, for his patient and constructive guidance during completion of the manuscript.

References

Aguilera, E., 1998. The Chalupas and Chachimbiro geothermal fields in Ecuador. Geotherm. Resour. Council Trans. 22, 247–251.

Almeida, E., Sandoval, G., Panichi, C., Noto, P., Bellucci, L., 1990. Modelo geotérmico preliminar de areas volcánicas del Ecuador a partir de estudios químicos e isotópicos de manifestaciones termales. Geothermal investigations with isotope and geochemical techniques in Latin America. In: IAEA-TECDOC-641. Proceedings of the Final Research Co-ordination Meeting held in San José, 12–16 November, Costa Rica.

Arnórsson, S., Gunnlaugsson, E., Svavarsson, H., 1983. The chemistry of geothermal waters in Iceland. II. Mineral equilibria and independent variables controlling water compositions. Geochim. Cosmochim. Acta 47, 547–566.

Berner, E.K., Berner, R.A., 1996. Global Environment: Water, Air, and Geochemical Cycles. Prentice Hall, Upper Saddle River.

Blank, J.G., Brooker, R.A., 1994. Experimental studies of carbon dioxide in silicate melts: solubility, speciation, and stable carbon isotope behaviour volatiles in magmas. In: Carroll, M.R., Holloway, J.R. (Eds.), Reviews in Mineralogy, 30, pp. 157–186.

Chiodini, G., Cioni, R., Guidi, M., Marini, L., 1991. Chemical geothermometry and geobarometry in hydrothermal aqueous solutions: a theoretical investigation based on a mineral-solution equilibrium model. Geochim. Cosmochim. Acta 55, 2709–2727.

Craig, H., Lupton, J.E., Horibe, Y., 1978. A mantle helium component in Circum-Pacific volcanic gases: Hakone, the Marianas, and Mt Lassen. In: Alexander, E.C., Ozima, M. (Eds.), In Terrestrial Rare Gases. Japan Sci. Soc. Press, pp. 3–16.

D'Amore, F., Panichi, C., 1980. Evaluation of deep temperature of hydrothermal systems by a new gas-geothermometer. Geochim. Cosmochim. Acta 44, 549–556.

Deines, P., Gold, D.P., 1973. The isotopic composition of carbonatite and kimberlite carbonates and their bearing on the isotopic composition of deep-seated carbon. Geochim. Cosmochim. Acta 37, 1709–1733.

Fournier, R.O., 1973. Silica in thermal waters: laboratory and field investigations. In: Proceedings of the International Symposium on Hydrogeochemistry and Biogeochemistry, Tokyo, pp. 122–139.

Fournier, R.O., 1977. Chemical geothermometers and mixing models for geothermal systems. Geothermics 5, 41–50.

Fournier, R.O., 1979. A revised equation for the Na/K geothermometer. Geotherm. Resour. Council Trans. 5, 1–16.

Fournier, R.O., Potter II., R.W., 1982. A revised and expanded silica (quartz) geothermometer. Geotherm. Resour. Council Bull. 11, 3–12.

Giggenbach, W.F., 1984. Mass transfer in hydrothermal alterations systems. Geochim. Cosmochim. Acta 48, 2693–2711.

Giggenbach, W.F., 1987. Redox processes governing the chemistry of fumarolic gas discharges from White Island. N. Z. Appl. Geochem. 2, 143–161.

Giggenbach, W.F., 1988. Geothermal solute equilibria derivation of Na–K–Mg–Ca geoindicators. Geochim. Cosmochim. Acta 52, 2749–2765.

Giggenbach, W.F., 1992. Isotopic shifts in waters from geothermal and volcanic systems along convergent plate boundaries and their origin. Earth Planet. Sci. Lett. 113, 495–510.

Giggenbach, W.F., 1993. Redox control of gas compositions in Philippine volcanic-hydrothermal systems. Geothermics 23, 575–587.

Henley, R.W., Ellis, A.J., 1983. Geothermal systems, ancient and modern: a geochemical review. Earth Sci. Rev. 19, 1–50.

Holloway, J.R., Blank, J.G., 1994. Application of experimental results to C–O–H species in natural melts. In: Carroll, M.R., Holloway, J.R. (Eds.), Volatiles in Magmas, Reviews in Mineralogy, 30, pp. 187–230.

Johnson, J.W., Oelkers, E.H., Helgeson, H.C., 1992. SUPCRT 92 A software package for calculating the standard molal thermodynamic properties of minerals, gases, aqueous species, and reactions from 1 to 5000 bars and 0 to 1000 °C. Comput. Geosci. 18, 899–947.

Kyser, T.K., 1986. Stable isotope variations in the mantle. In: Valley, J.W., Taylor Jr., H.P., O'Neil, J.R. (Eds.), Stable Isotopes in High Temperature Geological Processes, Reviews in Mineralogy, 16, pp. 141–164.

Mahon, W.A.J., Finlayson, J.B., 1972. The chemistry of the Broadlands geothermal area, New Zealand. Am. J. Sci. 272, 48–68.

Marini, L., Cioni, R., Guidi, M., 1998. Water chemistry of San Marcos area, Guatemala. Geothermics 27, 331–360.

Marini, L., Bonaria, V., Guidi, M., Hunziker, J.C., Ottonello, G., Vetuschi Zuccolini, M., 2000. Fluid geochemistry of the Acqui Terme-Visone geothermal area (Piemonte, Italy). Appl. Geochem. 15, 917–935.

McKenzie, W.F., Truesdell, A.H., 1977. Geothermal reservoir temperatures estimated from the oxygen isotope compositions of dissolved sulphate and water from hot springs and shallow drillholes. Geothermics 5, 51–61.

Ohmoto, H., Goldhaber, M.B., 1997. Sulfur and carbon isotopes. In: Barnes, H.L. (Ed.), Geochemistry of Hydrothermal Ore Deposits. Wiley, New York, pp. 517–612.

OLADE-AQUATER. Estudio de Prefactibilidad del Area de Tufiño. Anexos B y C, unpublished report.

OLADE-INECEL. Aprovechamiento de los Recursos Geotermicos de la Zona de Tufiño. Informe Hidrogeológico, unpublished report.

Pang, Z., 1992. Theoretical calibration of chemical geothermometers and its application to the granitic geothermal areas of SE China. In: Kharaka, Y.K., Maest, A.S. (Eds.), Water-Rock Interaction. Belkema, pp. 1463–1466.

Pang, Z., Reed, M.H., 1998. Theoretical chemical thermometry on geothermal waters: problems and methods. Geochim. Cosmochim. Acta 62 (6), 1083–1091.

Symonds, R.B., Rose, W.I., Bluth, G.J.S., Gerlach, T.M., 1994. Volcanic-gas studies: methods, results, and applications. In: Carroll, M.R., Holloway, J.R. (Eds.), Volatiles in Magmas, Reviews in Mineralogy, 30, pp. 1–60.

Thorpe, R.S., Francis, P.W., Hamill, M., Baker, M.C.W., 1982. In: Thorpe, R.S. (Ed.), The Andes. Andesites: Orogenic Andesites and Related Rocks. Wiley, Chichester, pp. 187–205.

Wilhelm, E., Battino, R., Wilcock, J., 1977. Low-pressure solubility of gases in liquid water. Chem. Rev. 77, 219–262.

Wohletz, K., Heiken, G., 1992. Volcanology and Geothermal Energy. University of California Press, Berkeley, Los Angeles, 432 pp.

Wolery, T. J., 1992. EQ3NR, a computer program for geochemical aqueous speciation–solubility calculations: theoretical manual, user's guide and related documentation (version 7.0). Report UCRL-MA-110662 PT III. Lawrence Livermore National Laboratory, Livermore, California.